

10 kV SiC MOSFET Power Module with Reduced Common-Mode Noise and Electric Field

Christina M. DiMarino, *Member, IEEE*, Bassem Mouawad, C. Mark Johnson, *Member, IEEE*,
Dushan Boroyevich, *Fellow, IEEE*, Rolando Burgos, *Member, IEEE*

Abstract—The advancement of silicon carbide (SiC) power devices with voltage ratings exceeding 10 kV is expected to revolutionize medium- and high-voltage systems. However, present power module packages are limiting the performance of these unique switches. The objective of this research is to push the boundaries of high-density, high-speed, 10 kV power module packaging. The proposed package addresses the well-known electromagnetic and thermal challenges, as well as the more recent and prominent electrostatic and electromagnetic interference (EMI) issues associated with high-speed, 10 kV devices. The high-speed switching and high voltage rating of these devices causes significant EMI and high electric field. Existing power module packages are unable to address these challenges, resulting in detrimental EMI and partial discharge that limit the converter operation. This paper presents the design and testing of a 10 kV SiC MOSFET power module that switches at a record 250 V/ns without compromising the signal and ground integrity due to an integrated screen reduces the common-mode current by ten times. This screen connection simultaneously increases the partial discharge inception voltage by more than 50 %. With the integrated cooling system, the power module prototype achieves a power density of 4 W/mm³.¹

I. INTRODUCTION

Wide-bandgap (WBG) semiconductors, such as silicon carbide (SiC), have demonstrated improved efficiency, reduced size and weight, and lower system cost compared to silicon [1],[2],[3],[4],[5]. SiC semiconductors have also demonstrated superior high-voltage capability [3],[4],[6]. While silicon devices have proven reliability and ruggedness, they have limited voltage ratings (typically 6.5 kV or less), thus requiring complex series connection of devices or multilevel converter topologies [7]. Moreover, medium-voltage silicon devices have slow switching speeds, which constrain the efficiency and switching frequency of the power converter [8],[9].

10 kV SiC MOSFETs are of great interest due to their high blocking voltage, fast switching speed, simple drivability, reverse conduction capability, and moderate on-state losses. These features can increase the efficiency, reliability, and

switching frequency, and reduce the complexity, size, and weight of medium- and high-voltage power conversion systems [10],[11]. Applications include electric ship propulsion [9],[13], data center distribution, direct renewable energy integration [14], fast charging stations [15], HVDC [16], FACTS [17],[18], and transformer-less intelligent substations [11],[14],[19],[20],[21].

Due to the vast possibilities for ≥ 10 kV SiC devices, significant resources have been devoted to their development. The majority of the reports on these devices have been focused on the characterization [6],[11],[19],[22],[23],[24], gate driver design [25],[26],[27],[28], and converter evaluation [11],[24],[29]. However, the packaging of the semiconductor dies has a significant impact on the performance, currently hindering their switching speed, voltage rating, current rating, and operating temperature. It is nontrivial to design a suitable package for 10 kV SiC MOSFETs. In addition to the well-known electromagnetic and thermal challenges associated with packaging WBG devices, the high voltage rating creates new and more prominent electrostatic and electromagnetic interference (EMI) issues, which need to be addressed to utilize the full capabilities of these devices.

The first-generation 10 kV SiC MOSFETs were assembled into a power module using a modified 6.5 kV silicon MOSFET package [30]. Upon analysis and testing of the power module, it was found that the parasitic inductances and capacitances were large and unbalanced [31], limiting the device performance and causing significant EMI. An improved package for third-generation 10 kV SiC MOSFETs is presented in [32]. This package has lower and more symmetrical parasitic inductances [32], though further improvement in the EMI is unknown.

EMI arises from the voltage and current transients occurring during operation of the switching cell, and is conducted through the electrical connections, or radiated into the surrounding space. Typically, filters are added to reduce the EMI; however, these increase the cost, size, and complexity of the power conversion system. Adding external filters diminishes the power density and some of the benefits gained by using 10 kV SiC MOSFETs.

In particular, conducted common-mode (CM) noise is a major issue with high-speed devices. CM noise is caused by the high-dv/dt switching of the semiconductor devices, which causes current to flow through the parasitic capacitances. These capacitances exist in the power module and at the system level, such as the gate driver isolation. The latter has

¹This work was supported in part by the UK Engineering and Physical Sciences Research Council (EPSRC) under grant EP/K035304/1 and the CPES High Density Integration Consortium.

C. DiMarino, D. Boroyevich, and R. Burgos are with Virginia Tech, Blacksburg, VA 24061 USA (e-mail: dimaricm@vt.edu, dushan@vt.edu, rolando@vt.edu).

B. Mouawad and C. M. Johnson are with the University of Nottingham, Nottingham NG7 2RD UK (e-mail: bassem.mouawad@nottingham.ac.uk, mark.johnson@nottingham.ac.uk).

addressed in other work by reducing the isolation capacitance of the gate driver power supply [25],[26],[27],[28].

To address the issue of current flowing through the parasitic capacitances within the package, [33] proposed a method for diverting the current back to the dc bus by using two stacked direct-bonded-copper (DBC) substrates, where the intermediate metal layer is connected to the positive or negative dc bus. The amount of current that is diverted will strongly depend on the high-frequency impedance of the connection back to the dc bus. Accordingly, the implementation of this screen is critical. In [33], wire bonds are used for the interconnections, and “lugs” are used for the terminals. These connection methods have large parasitic inductances, which will reduce the effectiveness of the screen.

In [34], a similar screen is proposed. The 1.2 kV SiC MOSFET power module in [34] uses a multilayer DBC substrate, and dc-link capacitors located close to the dies. Vias in the multilayer substrate create a low-inductance connection between the middle metal layer and the negative dc bus [34]. The module has a 14-dB reduction compared to the reference module [34],[35]. While this module has several advantageous features, there are some areas for improvement. First, by connecting the middle metal to the negative dc bus, as in [33], the top ceramic is providing all the voltage isolation, and thus the second ceramic is not being fully utilized. Second, by placing the capacitors on the same plane as the MOSFETs, the footprint of the module is significantly increased. Third, the module parasitics are not well balanced, which has been shown to cause greater high-frequency noise compared to balanced designs [36].

The high-voltage rating of the 10 kV SiC MOSFETs poses a challenge for the electrostatic performance. If the electric field exceeds the breakdown field strength of the insulation materials, such as the encapsulation or insulating substrate, then partial discharge (PD) can occur. Repetitive PD events can ultimately result in insulation failure, such as cracking of the ceramic substrate, as shown in [37], thus destroying the power module. Furthermore, the PD inception voltage (PDIV) has been shown to decrease with increased dv/dt and switching frequency [38]. Due to the high-speed switching capabilities of these 10 kV SiC MOSFETs, measures must be taken to reduce the electric field concentration within the power module to ensure sufficient PDIV and breakdown voltage.

In this work, an optimized high-voltage power module package was designed, prototyped, and tested using 10 kV SiC MOSFETs. With the proposed package, the 10 kV SiC MOSFETs are able to switch at record speeds with minimal ringing and voltage overshoot. This fast switching results in significantly reduced switching losses compared to medium-voltage silicon transistors, and allows the switching frequency of medium- and high-voltage converters to be increased by orders of magnitude, which drastically reduces the size of passive components, thereby increasing the system power density. To mitigate the conducted EMI that could result from this high dv/dt , this work proposes to fully integrate a low-inductance screen into the package that limits the amount of

CM current that flows out of the power module. In the implementation, the capacitors are arranged above the MOSFET switch pair to balance parasitic inductances, maintaining a small footprint. The middle metal layer is connected to the dc bus midpoint, which evenly distributes the electric field in the ceramic layers and reduces the electric field at the critical triple points. Thus, the proposed implementation will mitigate the CM current, while improving the voltage isolation, increasing the PDIV of the power module, and maintaining a small footprint for high power density.

In this paper, the EMI issues encountered during testing of the first-generation 10 kV SiC power modules from [33] will be presented, followed by a description of the proposed implementation for 10 kV SiC MOSFETs. The actual implementation, and preliminary testing of the integrated screen will then be discussed. Methods for reducing the electric field concentration within the power module will be reviewed, and the proposed technique will be analyzed. Finally, the experimental switching tests that demonstrate high-speed transients and low CM current of the proposed package will be presented. Partial discharge tests validating the improved voltage capability provided by the CM screen will also be shown.

II. EMI LIMITATIONS FOR HIGH-VOLTAGE SiC POWER MODULES

The development of 10 kV SiC MOSFETs [39] and 10 kV SiC junction barrier Schottky (JBS) diodes [40] gave rise to the first 10 kV SiC power module [30]. The half-bridge power modules comprise twelve parallel 10 kV, 10 A SiC MOSFETs, and six parallel 10 kV, 10 A SiC JBS diodes in a common switch position, yielding a current rating of 120 A [30]. The 10 kV SiC modules demonstrated higher efficiency and switching frequency potential than 6.5 kV silicon modules [8], and were critical components in the development of a high-density 1 MVA solid-state power substation. The modules employed soft switching techniques and were capable of switching up to 20 kHz [41]. These modules were also used to demonstrate the first medium-voltage impedance measurement unit (IMU) capable of characterizing in-situ source and load impedances of dc and ac networks up to 4160 V ac, 4160 V dc, 300 A, and 2.2 MVA [42]. Unfortunately, the full range of voltages and power levels could not be achieved due to significant conducted and unresolvable EMI. Upon further evaluation, it was found that a substantial current was flowing through the system ground. The contaminated ground was causing the control system to malfunction, thereby limiting the operating conditions.

As mentioned previously, under a voltage excursion, parasitic capacitances can become a path for CM current to flow. Within the power module, parasitic capacitances exist across the ceramic substrate that isolates the semiconductor devices from the cooling system. Since the cooling system is generally grounded for safety, under high-speed switching transients, this parasitic capacitance becomes a path for CM current to flow through the system ground [36]. Therefore,

capacitance should be minimized, especially for fast-switching devices.

From ANSYS Q3D simulations, the parasitic capacitance between the output node of the half-bridge and the module baseplate is approximately 300 pF. Discrete switching tests were conducted on these power modules to characterize the dynamic performance [43]. At 4.7 kV and 100 A, the power modules had a maximum dv/dt of 22 V/ns [43]. This measured dv/dt and simulated parasitic capacitance give a calculated peak current of nearly 7 A. It should be noted that the 22 V/ns switching speed was achieved with internal and external gate resistances slowing down the devices. If these resistances were reduced or eliminated, then the switching speed would increase, which would raise the efficiency, but worsen the CM current. Therefore, this capacitance is limiting the operation of the 10 kV SiC MOSFETs. The package proposed in this work reduces this EMI without sacrificing the efficiency by minimizing the parasitic capacitance, and integrating a screen that contains the generated CM current within the power module.

III. MODULE OVERVIEW

Fig. 1 shows the designed half-bridge power module, which has three 10 kV, 350 mΩ SiC MOSFET dies in parallel per switch position. No external anti-parallel diodes are used. The module has a planar, sandwich structure, using metal posts and direct-bonded-aluminum (DBA) substrates as the die interconnection instead of wire bonds. Similar structures were proposed in [44] and [45] for lower-voltage silicon IGBTs. This type of structure allows for increased power density, and reduces the parasitic inductances and capacitances in the module, thereby improving the dynamic performance. Furthermore, by eliminating the wire bonds, the module will be able to withstand higher-energy faults, as shown in [46]. This structure also allows decoupling capacitors to be embedded within the module to further improve the dynamic performance without increasing the module footprint.

In total, four substrates are used in the power module: two beneath the dies (DBA1 and DBA2) and two on top (DBA3 and DBA4). DBA1 and DBA2 are used to reduce the CM current flowing through the system ground and to decrease the peak electric field strength within the power module. With the housing and integrated cooler, the module dimensions are 70 mm × 80 mm × 25 mm. Details on the design and prototyping of this power module are reported in [47],[48],[49].

Fig. 2 shows two module prototypes: a low-current module with two dies (Fig. 2(a)), and a high-current module with six dies (Fig. 2(b)). The low-current module was fabricated to test the prototyping procedures, and was used for initial testing. The testing of these module prototypes will be presented in section VI.

IV. COMMON-MODE SCREEN

A. Impedance Analysis

In this section, the CM path impedances will be analyzed. Fig. 3 shows a schematic of the power module with the key impedances that will be considered. For the generated CM

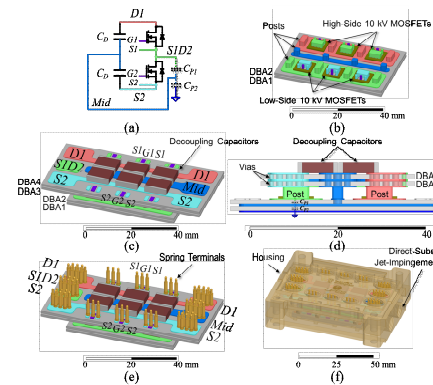


Fig. 1 (a) Schematic and 3D models of the (b) bottom and (c) top assemblies. (d) side-view of the module, (e) terminal arrangement housing with integrated cooler. The colors in the 3D models correspond to the nodes in the schematic with the same color.

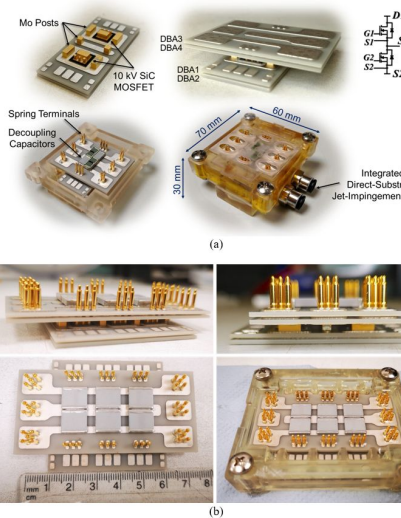


Fig. 2 10 kV SiC MOSFET module prototypes with (a) two 10 kV SiC MOSFET dies, and (b) six 10 kV SiC MOSFET dies.

current to be diverted from the ground to the screen, the impedance of the screen path must be much lower than the ground path, especially at high frequency. The condition required for the screen to effectively divert the CM current from the ground path to the dc bus may be summarized as follows:

$$Z_{screen} \ll Z_{gnd}$$

where Z_{screen} and Z_{gnd} are the impedances of the screen and ground paths, respectively. Considering the parasitic elements shown in Fig. 3, these impedances can be defined as:

$$Z_{screen} = \omega L_{screen} + 1/(j\omega C_D) + R_{screen} \quad (2)$$

$$Z_{gnd} = \omega L_{gnd} + 1/(j\omega C_{p2}) + R_{gnd} \quad (3)$$

where L_{screen} and L_{gnd} are the parasitic inductances in the screen and ground paths, R_{screen} and R_{gnd} are the parasitic resistances in the screen and ground paths, C_D is the decoupling capacitance, and C_{p2} is the parasitic capacitance of the bottom substrate, which is connected to ground (Fig. 1(d)). As shown by (2), to minimize Z_{screen} , L_{screen} should be as small as possible, while C_D should be large. From (3), it can be seen that a smaller C_{p2} results in a greater Z_{gnd} . Substituting (2) and (3) into (1) gives:

$$\omega L_{screen} + 1/(j\omega C_D) + R_{screen} \ll \omega L_{gnd} + 1/(j\omega C_{p2}) + R_{gnd} \quad (4)$$

From (4), it can be seen that the effectiveness of the screen is dependent on the parasitic elements, which are determined by the implementation. To effectively reduce the CM current, the power module should be compact such that C_{p2} and L_{screen} are small, yet capable of accommodating sufficient decoupling capacitance C_D . The L_{gnd} and R_{gnd} will vary depending on the system integration, and are therefore out of the control of the power module designer. Accordingly, this work focuses on minimizing C_{p2} and L_{screen} , and maximizing C_D . A more general theoretical analysis of CM impedances is presented in [50].

B. Preliminary Testing

Prior to constructing the 10 kV SiC MOSFET power modules, it was desirable to understand the effects of the proposed screen on the CM noise. Accordingly, a half-bridge module with 1.2 kV, 80 mΩ SiC MOSFETs (C2M0080120D) was built and tested in a boost converter. For the test, the module substrate was directly mounted onto a copper ground plane. No cooling system was added between the substrate and the ground plane to improve the measurement results. Due to the absence of a cooling system, the tests were conducted at

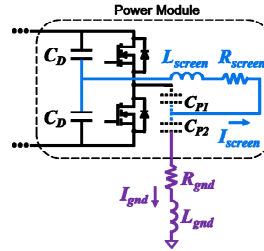


Fig. 3 Power module schematic with parasitic impedances of the ground (purple) and screen (blue) paths.

low power (360 W). The output voltage was 60 V, and the switching frequency was 50 kHz.

For the prototyped 1.2 kV SiC modules, the parasitic capacitance from the output node to the middle metal layer C_{p1} was 20 pF, and the parasitic capacitance from the metal layer to the ground, C_{p2} , was 150 pF. These values were measured on the prototype using an impedance analyzer and were verified by calculation and Q3D simulation. C_{p2} is larger than C_{p1} because the middle and bottom metal layers cover the entire substrate area, whereas the output terminal makes up a small portion of the footprint.

For the tests, a high-frequency current transformer (CT) was used to measure the current of the line impedance stabilization network (LISN). The output of the HFCT was connected to an EMC analyzer. The measured current waveforms are shown in Fig. 4. The first case has a single substrate and no decoupling capacitors. The second case has two stacked substrates and no decoupling capacitors. The third case has two stacked substrates and two 680-pF decoupling capacitors in parallel and two in series, but the middle metal layer of the substrate stack is left floating. The fourth case is similar to the third, but has two series 10-nF capacitors. The fifth case connects the middle metal layer of the substrate stack to the midpoint of the series decoupling capacitors.

When two substrates are stacked together (case 2), the CM noise decreases by just a few dB compared to case 1 with a single substrate. This indicates that the reduction in the parasitic capacitance offered by the second substrate is not sufficient to lower the CM noise. The addition of 680-pF decoupling capacitors in case 3, on the other hand, reduces the CM noise frequency noise by more than 10 dB compared to case 1 with a single substrate. The decoupling capacitors also cause the resonant frequency to decrease. When the decoupling capacitance is increased to 10 nF (case 4), then the resonant frequency further decreases, and the high-frequency noise is reduced by a few more dB. This is in agreement with the expectation, which shows that increasing the decoupling capacitance helps to reduce the high-frequency impedance of the screen. When the middle metal of the substrate stack is connected to the midpoint of the two series 10-nF capacitors (case 5), the high-frequency noise decreases by more than 15 dB in the larger frequency range. This is because there is now a low impedance, high-frequency path for the generated CM current to flow. This preliminary testing demonstrates the potential of the screen to reduce the CM noise.

The gate-source and drain-source voltages and drain current of the 1.2 kV SiC MOSFET were also monitored during testing. By adding decoupling capacitors, the high-frequency noise in the drain-source voltage reduced, and the ringing was decreased, resulting in greater current overshoot and amplitude ringing. This ringing and overshoot can be reduced by decreasing the power-loop inductance, which was optimized in this module prototype. Connecting the middle metal layer to the decoupling capacitor midpoint did not result in noticeable changes in the MOSFET voltage and current waveforms. Therefore, if the parasitic inductances and

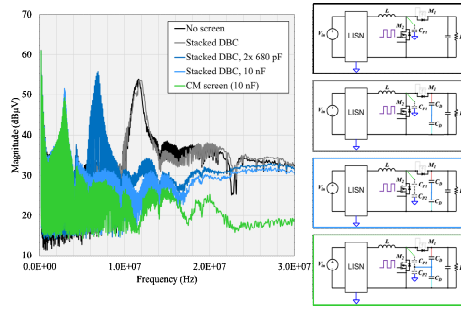


Fig. 4 Measured LISN current in 1.2 kV-SiC-based boost converter with (green waveform) and without (black, grey, and blue waveforms) the proposed CM screen.

decoupling capacitors are carefully designed, the proposed CM screen will have minimal impact on the MOSFET losses.

C. Implementation

To achieve a low-impedance implementation for the CM screen in the 10 kV power module, it is proposed to embed capacitors, and to use vias within the insulating ceramic substrates to make the connection between the middle metal layer and the capacitor potentials. In [50], the capacitors are placed above the semiconductor devices, creating a vertical high-frequency power loop that does not increase the module footprint, as it takes advantage of the third dimension. In this work, this vertical-capacitor-loop concept was adopted with some modifications. Each 10 kV SiC MOSFET switch pair has its own set of decoupling capacitors located above it (Fig. 1(c)), resulting in a symmetric power loop inductance of just 4.4 nH for each. In this embodiment, two capacitors are placed in series, and the midpoint, which is at half of the dc bus voltage, is connected to the middle metal of the substrate stack. By connecting the screen to the decoupling capacitors within the power module, the influence of the parasitic impedances external to the package are diminished thereby improving the effectiveness of the screen.

According to ANSYS Q3D simulations, this connection method has less than 2 nH parasitic inductance, allowing for a high proportion of the CM current to be diverted to the dc bus and contained within the power module. Additionally, the SID2 pad area was designed as small as possible to minimize C_{P1} . For the proposed high-current 10 kV power module shown in Fig. 1 and Fig. 2(b), C_{P1} is 46 pF, and C_{P2} is 160 pF, according to ANSYS Q3D simulations. For the decoupling capacitors (C_D), a surface-mount, 680 pF, COG, 5 kV multilayer ceramic capacitor was selected. As shown in Fig. 1(c), there are three capacitors in parallel—one above each MOSFET switch pair—giving an equivalent capacitance of 2.04 nF.

V. ELECTRIC FIELD REDUCTION

To address the enhanced electric field associated with high-voltage, high-density package, the ceramic substrate must be thoughtfully designed and evaluated. In power modules, the electric field concentrates at the interfaces between the ceramic, metal, and encapsulation [52],[53],[54],[55]. This is known as the triple point. If this electric field exceeds the breakdown field strength of the insulation materials, partial discharge (PD) can occur. If the PD occurs in the ceramic or encapsulation, then PD can occur. Repeated PD events can ultimately result in insulation failure, cracking of the ceramic substrate as shown in [37], and eventually destroying the power module.

In the literature, it has been shown that the PD rate for a standard 1-mm-thick aluminum nitride (AlN) DBC substrate is less than 10 kV rms [37], and can be as low as 5 kV rms [56]. This does not provide sufficient margin for 10 kV SiC MOSFETs. Accordingly, methods for reducing the electric field within the power module need to be explored. There have been several proposed solutions to reduce the electric field strength at the triple point, including: increasing the ceramic thickness [37]; varying the metal pad size and pad corner curvature [37], offset between the top and bottom metal pads [37], and metal-ceramic interface geometry [57],[58],[59]; and stacking multiple substrates [56]. None of these previously proposed solutions were implemented and tested in an actual power module, and several of the methods complicate the module manufacturing. The method proposed in this work, is an adaptation of the latter method and effectively increases the PDIV, and is simple to implement.

In [56], it was shown that stacking DBC substrates reduces the electric field strength within the bulk ceramic at the critical triple points. The PD tests revealed that the PDIV could be increased by 94 % by stacking two 0.5 mm Al₂O₃ substrates compared to having a single 0.5 mm substrate [56]. However, the practical implementation of this method was not explored. In a power module, the top and bottom metal layers are not symmetrical; the top metal is patterned to create the circuit (e.g., half bridge), and various traces are at different potentials during the normal operation. As a result, it is not clear what potential should be applied to the middle metal layer to achieve a meaningful reduction in the electric field strength. This key factor in the realization of this method is explored in this work.

Fig. 5 shows the simulated 2D electric field distribution for the case when the top metal is patterned and has different potentials. One of the potentials represents the positive dc bus potential while the other represents the drain of the high-side switch, and the other represents the drain of the low-side switch. The former is consistently at the positive dc bus potential while the latter switches between the positive and negative dc bus potentials. The worst-case scenario occurs when the low-side switch is conducting and its drain is at the negative dc bus potential. This worst-case was simulated with the positive dc bus is set to 10 kV, and the negative is set to 0 V. The bottom-most metal is at the same potential as the top metal system, which is grounded (0 V).

Fig. 5(a) shows the simulated electric field plot for a single DBA substrate. It can be seen that the electric

distribution is non-uniform within the bulk of the ceramic, and that the peak electric field occurs at the triple points. The peak electric field exceeds 20 kV/mm, which is the typical breakdown field strength for ceramic substrates.

Fig. 5(b) shows the simulated electric field plot for two stacked DBA substrates with the middle metal layer connected to the negative dc bus (0 V), as proposed in [33] and [34]. Comparing Fig. 5(a) and Fig. 5(b), it can be seen that connecting the middle metal to the negative dc bus does not reduce the peak electric field at the triple point, nor does it improve the distribution within the bulk ceramic, compared to the single substrate case. This is because the bottom substrate has 0 V across it, while the top substrate has 10 kV. In this implementation, the bottom substrate is not helping to support the voltage, and is therefore not being fully utilized.

If the middle metal is connected to the positive dc bus, as proposed in [33], then the triple points at which the peak electric field occur will change, and the electric field distribution within the bulk ceramic will shift. This is shown in Fig. 5(c). Although the distribution and critical triple points have changed, the peak electric field, and therefore the PDIV, are similar to the case with a single substrate. This is because both the top and bottom substrates have 10 kV across them.

If instead the middle metal is connected to half of the applied voltage, then both the top and bottom substrates have a potential of 5 kV across them. The simulated electric field distribution for this case is shown in Fig. 5(d). The simulated peak electric field is reduced by 58 % compared to the single-substrate case (Fig. 5(a)), and the electric field in the bulk ceramic is uniformly distributed in the two substrates. Therefore, in this work, the middle metal layer of the DBA stack is connected to half of the bus voltage.

The connection of the middle metal layer to half of the bus potential can be realized with the embedded decoupling capacitors. Each set of decoupling capacitors shown in Fig. 1(c) consists of two, 5 kV ceramic capacitors placed in series. From Fig. 1(d), it can be seen that the midpoint of the capacitors is connected to the middle metal layer of the bottom DBA stack through vias and metal posts. This connection allows the middle metal layer to be connected to half of the bus voltage, thus reducing the peak electric field in the power module.

VI. EXPERIMENTAL RESULTS

A. Switching Testing

To evaluate the switching performance of the proposed 10 kV power module, double-pulse tests (DPT) were performed on the low-current prototype shown in Fig. 2(a). The DPT schematic and setup are shown in Fig. 6. The gate driver used for the DPTs was adapted from the one presented in [60]. The low-side 10 kV SiC MOSFET was driven from +20 V in the on-state to -5 V in the off-state. The body diode of the high-side 10 kV SiC MOSFET was used as the free-wheeling

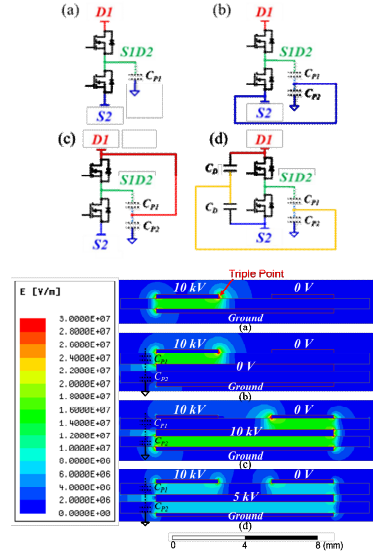


Fig. 5 Simulated 2D electric field distribution for (a) a single substrate and two stacked substrates with the middle metal at the (b) negative dc bus, (c) positive dc bus, and (d) dc bus midpoint.

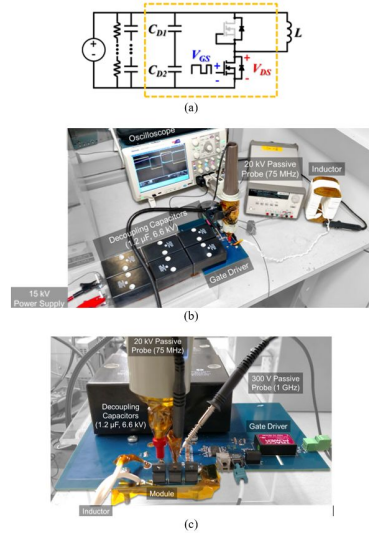


Fig. 6 Double-pulse test (a) schematic with the power module indicated by the yellow box, (b) hardware setup, and (c) module connection.

diode. The gate driver PCB is mounted on top of the power module to achieve small gate-loop inductance between the driver and the module.

The gate-source and drain-source voltages of the low-side SiC MOSFET were monitored using a 300 V passive probe with a bandwidth of 1 GHz, and a 20 kV passive probe with a bandwidth of 75 MHz, respectively. As shown in Fig. 6(c), these probes are placed directly above the MOSFET terminals to minimize the parasitic inductance in the measurement loop. Due to the embedded decoupling capacitors, the drain current of the SiC MOSFETs could not be measured. A 15 kV power supply was used to charge the external decoupling capacitors. Each capacitor is 0.82 μF and rated at 3.3 kV (MP80CV824K [61]). Six total capacitors were used—two in series and three in parallel for a total capacitance of 1.2 μF and voltage rating of 6.6 kV. Three capacitors were put in parallel to increase the capacitance and to reduce the inductance; each capacitor has an equivalent series inductance of 30 nH [61].

Fig. 7 shows the gate-source and drain-source voltage waveforms for the turn-on and turn-off transients for the DPTs performed on the module shown in Fig. 2(a). The switching tests were performed up to 5 kV and 20 A with turn-on and turn-off gate resistances of 0.33 Ω and 0.17 Ω , respectively. Table I lists the measured overshoot, undershoot, rise and fall times, and switching rates from the DPTs. During the turn-on transient, the fall time of the drain-source voltage is 16 ns, giving a dv/dt of 250 V/ns. At turn-off, the voltage rise time is 50 ns, which is a dv/dt of 80 V/ns. The voltage rise time is longer because it is controlled by the output capacitance and load current. Negligible voltage overshoot and ringing were measured, indicating low power- and gate-loop inductances. This is due to the low-inductance module design, as well as careful layout and connection of the gate driver, bus bar, external decoupling capacitors, and measurement probes.

To the best of the author's knowledge, these are the fastest switching speeds reported for similarly-rated SiC MOSFETs and IGBTs. In fact, this is more than two times faster than those reported in [24],[32],[62],[63]. In [32], switching results for a module populated with a single die had turn-on and turn-off transition times of approximately 80 ns and 120 ns, respectively, giving switching speeds of 88 V/ns and 58 V/ns at a bus voltage of 7 kV, drain current of 15 A, and gate resistance of 21 Ω . The switching waveforms also showed a moderate voltage overshoot of approximately 300 V (4.3 %) [32].

For a discrete 4 kV silicon IGBT, the datasheet reports voltage rise and fall times of 146 ns and 514 ns at 1.25 kV, 30 A, and 2 Ω external gate resistance [64]. These switching times result in dv/dt values of 8.6 V/ns and 2.4 V/ns for the rise and fall, respectively, which are 10 and 100 times slower than the switching speeds achieved in this work. Accordingly, the proposed power module can enable faster-switching, higher-voltage power converters while maintaining high efficiency.

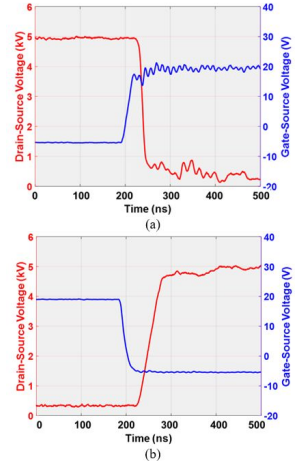


Fig. 7 (a) Turn-on and (b) turn-off gate-source (blue, right axis) and drain-source (red, left axis) voltages.

TABLE I
10 kV, 350 m Ω SiC MOSFET Module Prototype Switching Res

Parameter	Value	
	Gate-Source Voltage	Drain-Source Voltage
Overshoot	None	None
Undershoot	None	None
Rise Time	24 ns	50 ns
Rise dv/dt	0.9 V/ns	80 V/ns
Fall Time	26 ns	16 ns
Fall dv/dt	0.8 V/ns	250 V/ns

B. Common-Mode Screen Testing

To evaluate the effectiveness of the integrated CM screen on the 10 kV power module, switching tests were performed. As mentioned earlier, the CM current increases as the dv/dt and parasitic capacitances increase. To improve the signal-to-noise ratio of the CM current measurement, the test voltage was reduced. This was achieved by lowering the test voltage to 2 kV. To ensure sufficient CM current could be measured, the larger power module with three 10 kV SiC MOSFET dies in parallel per switch position was used [65]. The C_{p1} and C_{p2} of this 10 kV prototype are 100 pF and 162 pF, respectively.

Fig. 8(a) shows the schematic of the tests when the CM screen is not connected (the middle metal layer of the substrate stack is floating). Fig. 8(b) shows the schematic of the tests when the CM screen is connected to the common midpoint. An inductor with high-voltage wire for the winding was connected across the high-side switch of the half-bridge module. The body diode of the high-side SiC MOSFET was used to freewheel the current in the inductor when the high-side switch was off.

To validate the performance of the CM screen, the common-mode current I_{gnd} through the ground path, I_{gnd} , was measured, as shown in

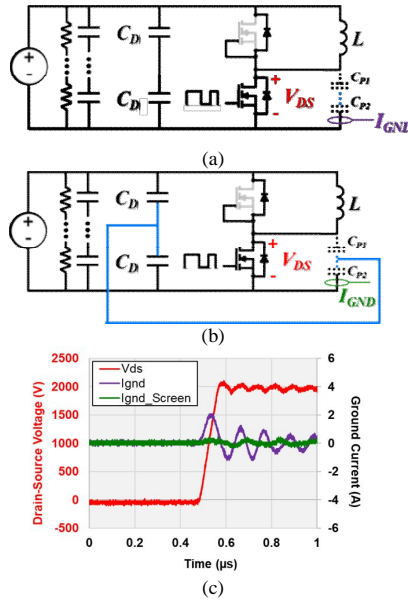


Fig. 8 Schematic of the testing setup when the screen is (a) not connected and (b) connected, and (c) drain-source (red, left axis) and ground current (right axis) waveforms with (green) and without (purple) the common-mode screen.

8, using an RF current transformer with a bandwidth of 200 MHz. For these tests, the middle metal layer was connected to the midpoint of the two series 680-pF decoupling capacitors. Three capacitors were placed in parallel.

Fig. 8(c) shows the turn-off drain-source voltage and ground current waveforms with and without the screen at 2 kV and 20 A with no external gate resistance. The voltage rise time at turn off is 66 ns, which gives a dv/dt of 24 V/ns. This dv/dt is lower than the previous switching tests because of the lower bus voltage and larger device capacitance due to the three MOSFET dies in parallel. The measured peak current through the ground path without the proposed screen is 2 A. This peak current will increase as the dc bus voltage, and therefore the dv/dt , increases. With the CM screen connected, the measured peak current through the ground path is reduced to 0.2 A. This is an order of magnitude reduction.

C. Partial Discharge Testing

PD tests were conducted to validate the electrostatic simulation results. The PD tests were performed using a 50 kV, 100-mA, 60-Hz power supply as the excitation source. To detect the PD events, a Doble PD Smart with HFCT-300 sensor was used [66]. The Doble PD Smart complies with IEC 60270 and VDE 0434, among other standards [66]. PD signals at frequencies from 35 kHz to 20 MHz and an apparent charge as low as 0.2 pC can be measured [66].

PD tests were performed on a patterned, 1-mm-thick DBA substrate. The spacing between metal traces and the metal traces to the edge of the ceramic was 2 mm. Three cases were tested: 1) a single substrate, 2) two substrates with the middle metal connected to the source ground, and 3) two stacked substrates with the middle metal connected to half of the applied excitation voltage. Each case was tested under two conditions: 1) SID2= D1 (the high-side switch is conducting and the low-side switch is blocking) and 2) SID2= S2 (the high-side switch is blocking and the low-side switch is conducting).

First, the PD tests were performed with the sample in air to have a high signal-to-noise ratio. These tests revealed that, as was shown in the electrostatic simulations, the PD events on DBA substrates will occur at the triple points. Specifically, a PD will take place along the edge of the metal pad where the high potential is applied. The resulting PDIV for the samples when the samples are tested in air are listed in Table II. For SID2 is equal to D1 (the applied voltage), and the middle metal is connected to half of the applied voltage, the measured PDIVs for this sample are listed in Table II. The same increase in PDIV was observed when SID2 is equal to S2 (ground). These results, which are in good agreement with the simulations, demonstrate that connecting the middle metal to half of the applied voltage gives predictable and consistent results for both switching states.

Since the power module will be encapsulated, PD tests were also performed on a stacked substrate sample that was encapsulated with SilGel 612 from Wacker. For this case, the SID2 potential was connected to S2 (the worst case). The measured PDIVs for this sample are listed in Table II. For the middle metal is connected to the source ground, the measured PDIV is 7.4 kV rms (10.5 kV peak). For this same case, a breakdown occurred at 8.5 kV rms (12.0 kV peak). This means that if the middle metal is connected to ground, or if a single substrate is used, then there is 20 % margin between the peak breakdown voltage and the voltage rating of the 10 kV SiC MOSFET. When the middle metal is connected to half of the applied voltage, no PD could be measured up to 10.5 kV rms (14.7 kV peak). The testing was stopped at 10.5 kV rms due to a reduced signal-to-noise ratio. This suggests that encapsulating stacked substrates with the middle metal connected to half of the applied voltage will have more than a 40 % higher PDIV.

TABLE II
Partial Discharge Testing Summary

Sample	Voltage of Middle Metal	Surrounding Medium	SID2 Potential	PDIV (rms)
Single Substrate	N/A	Air	D1	1.7 kV
Single Substrate	N/A	Air	S2	1.7 kV
Stacked Substrates	$\frac{1}{2} \times V_{AC}$	Air	D1	2.6 kV
Stacked Substrates	$\frac{1}{2} \times V_{AC}$	Air	S2	2.6 kV
Encapsulated Stacked Substrates	0 V	SilGel 612	S2	7.4 kV
Encapsulated Stacked Substrates	$\frac{1}{2} \times V_{AC}$	SilGel612	S2	>10.5 kV

compared to a single substrate or a stacked substrate with the middle metal connected to ground. Therefore, it is advantageous to use the stacked substrate structure with the middle metal connected to half the applied voltage to increase the high-voltage performance of the power module.

VII. CONCLUSIONS

This work proposed a high-density power module for 10 kV SiC MOSFETs with reduced CM current and electric field strength. The optimal layout and system interface enable the module to switch 5 kV in tens of nanoseconds with negligible ringing and voltage overshoot. This is the fastest switching speed reported to date for 10 kV SiC MOSFETs. To reduce the adverse EMI effects of this high-speed switching, a CM screen was incorporated into the power module design. This screen was realized by stacking two DBA substrates and connecting the middle metal to the midpoint of embedded decoupling capacitors through vias and metal posts. This proposed method creates a low-impedance path at high frequency, and contains the current that would normally flow to the system ground within the power module. With this screen, the measured CM current leaving the power module decreases by ten times. This proposed integrated screen will reduce the need for filtering at the system level, thereby increasing the power density, lowering the cost, and simplifying the design of power electronic systems. Moreover, it will permit the operation of the 10 kV SiC MOSFETs at faster speeds, thereby reducing losses and increasing efficiency.

This screen also increases the voltage rating of the power module. PD tests showed that stacking two substrates and connecting the middle metal to half of the applied voltage increases the PDIV by 53 % compared to a single substrate. When testing two encapsulated stacked substrates with the middle metal connected to the source ground, breakdown occurred at 8.5 kV rms (12.0 kV peak). This breakdown voltage limits the voltage rating of the package. When the middle metal of the encapsulated substrates is connected to half of the applied voltage, the PDIV exceeds 10.5 kV rms. This method for reducing the electric field is effective and simple to implement, and will enable high-voltage packages with greater power density.

ACKNOWLEDGMENT

The authors would like to acknowledge the experimental assistance from Ke Li and Yue Xu. The authors also acknowledge the assistance of Dr. Xiangyong Feng and the Center for Electromechanics at the University of Texas at Austin in conducting the partial discharge tests. The substrates used in the power module prototypes were donated by DOWA, and the external decoupling capacitors used for the switching tests were donated by Electronic Concepts. This work was funded in part by the UK Engineering and Physical Sciences Research Council (EPSRC) through research grant [EP/K035304/1] and the CPES High Density Integration

Consortium. This work was conducted with the use of ANSYS Maxwell 2D, ANSYS Maxwell 3D, and ANSYS Extractor, donated in-kind by Ansoft Corporation of the Industry Partnership Program.

REFERENCES

- [1] H. Zhang, L. M. Tolbert, B. Ozpineci, "Impact of SiC diode on hybrid electric and plug-in hybrid electric vehicles," *IEEE Ind. Appl.*, vol. 47, no. 2, pp. 912-921, Mar.-Apr. 2011.
- [2] A. Bindra, "SiC-based PV inverters display reduced size and cost," *How2Power Today*, May 2013.
- [3] J. Rabkowski, D. Pefitsis, H. P. Nee, "Silicon carbide transistors- A new era in power electronics is initiated," *IEEE Electron. Mag.*, vol. 6, no. 2, pp. 17-26, June 2012.
- [4] J. Millan, P. Godignon, X. Perpina, A. Perez-Tomas, J. "A survey of wide bandgap power semiconductor devices," *Trans. Power Electron.*, vol. 29, no. 5, pp. 2155-2163, May 2015.
- [5] "Train trial shows a 40 % energy saving for SiC inverters," *IEEE Electron. Mag.*, June 2015.
- [6] J. W. Palmour, L. Cheng, V. Pala, E. V. Brunet, Lichtenwalner, G. Y. Wang, J. Richmond, M. O'Loughlin, S. T. Allen, A. A. Burk, C. Scozzie, "Silicon carbide MOSFETs: Breakthrough performance from 900 V up to 10 kV," in *IEEE International Symposium on Semiconductor Device Research and IC's*, June 2014.
- [7] T. Lu, Z. Zhao, S. Ji, H. Yu, L. Yuan, "Parameter design of a balancing circuit for series connected HV-IGBTs," in *International Power Electronics and Motion Control Conference*, June 2012.
- [8] H. Mirzaee, A. De, A. Tripathi, S. Bhattacharya, "Comparison of high-power medium-voltage converters based on 6.5-kV Si-IGBT/Si-PiN diode, a 6.5-kV Si-IGBT/SiC-JEBS diode and a 10-kV SiC-MOSFET/SiC-JBS diode," *IEEE Trans. Appl.*, vol. 50, no. 4, July/Aug. 2014.
- [9] J. Casarin, P. Ladoux, P. Lasserre, "10kV SiC MOSFET based 6.5kV Si-IGBTs for medium frequency transformer application in railway traction," in *IEEE International Conference on Systems for Aircraft, Railway, Ship Propulsion, and Road Vehicle*, Mar. 2015.
- [10] K. Hatua, S. Dutta, A. Tripathi, S. Baek, G. Karimi, S. Bhattacharya, "Transformer less intelligent power substations design with 15kV SiC IGBT for grid interconnection," in *IEEE Energy Conversion Congress and Exposition*, Sept. 2011.
- [11] S. Madhusoodhanan, A. Tripathi, D. Patel, K. Mainali, A. Kadavelugu, S. Hazra, S. Bhattacharya, K. Hatua, "Solid state transformer and MV grid tie applications enabled by 15 kV SiC IGBTs and 10 kV SiC MOSFETs based multilevel converter," *IEEE Trans. Ind. Appl.*, vol. 51, no. 4, pp. 3343-3360, Aug. 2015.
- [12] "IEEE Recommended Practice for 1 kV to 35 kV Medium Voltage DC Power Systems on Ships," IEEE Standard 1709-2010, Nov. 2010.
- [13] C. Zhao, D. Dujic, A. Mester, J. K. Steinke, M. Weiss, S. I. Schmid, T. Chaudhuri, P. Stefanutti, "Power electronic transformer- Medium voltage prototype," *IEEE Trans. Electron.*, vol. 61, no. 7, pp. 3257-3268, Aug. 2013.
- [14] D. C. Patel, A. Kadavelugu, S. Madhusoodhanan, S. Bhatnagar, K. Hatua, S. Leslie, S. H. Ryu, D. Grider, A. Agarwal, "10 kV IGBT based three-phase three-level modular-leg power converter," in *IEEE Energy Conversion Congress and Exposition*, Sept. 2016.
- [15] S. Srdic, X. Liang, C. Zhang, W. Yu, S. Lukic, "A SiC-based performance medium-voltage fast charger for plug-in electric vehicles," in *IEEE Energy Conversion Congress and Exposition*, Sept. 2016.
- [16] M. S. Chinthavali, L. M. Tolbert, B. Ozpineci, "4H-SiC G thyristor and p-n diode loss models for HVDC converter," in *Industry Applications Conference*, Oct. 2004.
- [17] Y. Koyama, Y. Nakazawa, H. Mochikawa, A. Kuzumaki, N. Okada, "A transformerless 6.6-kV STATCOM based on SiC MOSFETs," in *IEEE Energy Conversion Congress and Exposition*, Sept. 2016.

- hybrid cascade multilevel converter using SiC devices," in *IEEE Trans. Power Electron.*, vol. 33, no. 9, pp. 7411-7423, Nov. 2017.
- [18] P. Wolfs, F. Yang, Q.-L. Han, "Distribution level SiC FACTS devices with reduced dc bus capacitance for improved load capability and solar integration," in *IEEE International Symposium on Industrial Electronics*, June 2014.
- [19] M. K. Das, C. Capell, D. E. Grider, S. Leslie, J. Ostrop, R. Raju, M. Schutten, J. Nasadoski, A. Hefner, "10 kV, 120 A SiC half H-bridge power MOSFET modules suitable for high frequency, medium voltage applications," in *IEEE Energy Conversion Congress and Exposition*, Sept. 2011.
- [20] R. Chattopadhyay, S. Bhattacharya, N. C. Foureaux, S. M. Silva, F. Braz Cardoso, H. de Paula, I. A. Piers, P. C. Cortizio, L. Moraes, J. A. de S. Brito, "Low-voltage PV power integration into medium voltage grid using high-voltage SiC devices," in *International Power Electronics Conference*, May 2014.
- [21] A. Q. Huang, Q. Zhu, L. Wang, L. Zhang, "15 kV SiC MOSFET: An enabling technology for medium voltage solid state transformers," *CPSS Trans. Power Electron. Appl.*, vol. 2, no. 2, pp. 118-130, Aug. 2017.
- [22] V. Pala, E. V. Brunt, L. Cheng, M. O'Loughlin, J. Richmond, A. Burk, S. T. Allen, D. Grider, J. W. Palmour, "10 kV and 15 kV silicon carbide power MOSFETs for next-generation energy conversion and transmission systems," in *IEEE Energy Conversion Congress and Exposition*, Sept. 2014.
- [23] M. Das, C. Capell, D. Grider, S. Leslie, J. Ostrop, R. Raju, M. Schutten, J. Nasadoski, A. Hefner, "10 kV, 20 A SiC half H-bridge power MOSFET modules suitable for high frequency, medium voltage applications," in *IEEE Energy Conversion Congress and Exposition*, Sept. 2011.
- [24] K. Vechalapu, S. Bhattacharya, E. Van Brunt, S.-H. Ryu, D. Grider, J. W. Palmour, "Comparative evaluation of 15-kV SiC MOSFET and 15-kV SiC IGBT for medium-voltage converter under the same dv/dt conditions," in *IEEE J. Emerging Sel. Topics Power Electron.*, vol. 5, no. 1, pp. 469-489, Mar. 2017.
- [25] A. Kadavelugu, "Medium voltage power conversion enabled by 15 kV SiC IGBTs," Ph.D. dissertation, North Carolina State Univ., NC, 2015.
- [26] X. Zhang, H. Li, J. A. Brothers, L. Fu, M. Perales, J. Wu, J. Wang, "A gate drive with power over fiber-based isolated power supply and comprehensive protection functions for 15-kV SiC MOSFET," *IEEE J. Emerging Sel. Topics Power Electron.*, vol. 4, no. 3, pp. 946-955, Sept. 2016.
- [27] A. Tripathi, K. Mainali, S. Madhusoodhanan, A. Yadav, K. Vechalapu, S. Bhattacharya, "A MV intelligent gate driver for 15kV SiC IGBT and 10kV SiC MOSFET," in *IEEE Applied Power Electronics Conference and Exposition*, Mar. 2016.
- [28] D. Berning, T. Duong, J. Ortiz-Rodriguez, A. Rivera-Lopez, A. Hefner, "High-voltage isolated gate drive circuit for 10 kV, 100 A SiC MOSFET/JBS power modules," in *IEEE IAS Annual Meeting*, pp. 1-7, 2008.
- [29] S. Moballegh, S. Madhusoodhanan, S. Bhattacharya, "Evaluation of high voltage 15 kV SiC IGBT and 10 kV SiC MOSFET for ZVS and ZCS high power DC-DC converters," in *International Power Electronics Conference*, May 2014.
- [30] M. Das, D. Grider, S. Leslie, R. Raju, M. Schutten, A. Hefner, "10 kV SiC power MOSFETs and JBS diodes: enabling revolutionary module and power conversion technologies," *J. Mat. Sci. Forum*, vol. 717-720, pp. 1225-1228, May 2012.
- [31] Z. Chen, R. Burgos, D. Boroyevich, F. Wang, S. Leslie, "Modeling and simulation of 2 kV 50 A SiC MOSFET/JBS power modules," in *IEEE Electric Ship Technol. Symp.*, Apr. 2009.
- [32] B. Passmore, Z. Cole, B. McGee, M. Wells, J. Stabach, J. Bradshaw, R. Shaw, D. Martin, T. McNutt, E. VanBrunt, B. Hull, D. Grider, "The next generation of high voltage (10 kV) silicon carbide power modules," in *IEEE Workshop on Wide Bandgap Power Devices and Applications*, Nov. 2016.
- [33] D. Domes, "Semiconductor arrangement," U.S. Patent 2013/0043593 A1, Feb. 21, 2013.
- [34] T. Huber, A. Kleimaier, S. Polster, O. Mathieu, "Low inductive SiC power module design using ceramic multilayer substrates," in *International Exhibition and Conference for Power Electronics, Intelligent Motion, Renewable Energy and Energy Management*, June 2018.
- [35] T. Huber, A. Kleimaier, R. Kennel, "Ultra-low inductive power module design with integrated common mode noise shield," *European Conference on Power Electronics Applications*, 2017.
- [36] A. Domurat-Linde, E. Hoene, "Analysis and reduction of EMI of power modules," in *International Conference on Integrated Power Electronics Systems*, Mar. 2012.
- [37] C. Bayer, U. Waltrich, R. Schneider, A. Soueidan, E. Schletz, "Enhancing partial discharge inception voltage by geometrical variations based on simulations of the electric strength," in *International Conference on Integrated Power Electronics Systems*, Mar. 2016.
- [38] P. Wang, A. Cavallini, G. C. Montanari, "The influence of repetitive square wave voltage parameters on enameled wire endurance," *IEEE Trans. Dielectr. Electr. Insul.*, vol. 21, no. 12, pp. 1276-1284, June 2014.
- [39] S. H. Ryu, S. Krishnaswami, B. Hull, J. Richmond, A. Ag. Hefner, "10 kV, 5 A 4H-SiC power DMOSFET," in *International Symposium on Power Semiconductor Devices and IC's*, 2006.
- [40] B. A. Hull, J. J. Sumakeris, M. J. O'Loughlin, Q. Zhang, J. Richmond, A. R. Powell, E. A. Imhoff, K. D. Hobart, A. Lopez, A. R. Hefner, "Performance and stability of large SiC 10-kV junction barrier Schottky rectifiers," *IEEE Electron. Devices*, vol. 55, no. 8, pp. 1864-1870, 2008.
- [41] D. Grider, M. Das, R. Raju, M. Schutten, S. Leslie, J. Ostrop, A. Hefner, "10 kV/120 A SiC DMOSFET half H-bridge modules for 1 MVA solid state power substation," *Electric Ship Technologies Symposium*, pp. 131-134, 2011.
- [42] M. Jaksic, Z. Shen, I. Cvetkovic, D. Boroyevich, R. Burgos, D. Marino, F. Chen, "Medium-voltage impedance measurement unit for assessing the system stability of electric ships," *Trans. Energy Convers.*, vol. 32, no. 2, pp. 829-841, Apr. 2017.
- [43] C. DiMarino, I. Cvetkovic, Z. Shen, R. Burgos, D. Boroyevich, "10 kV, 120 A SiC MOSFET modules for a power electronic building block (PEBB)," in *IEEE Workshop on Wide Bandgap Power Devices and Applications*, Oct. 2014.
- [44] S. Haque, K. Xing, R. L. Lin, C. T. A. Suchicital, G. Q. Nelson, D. Boroyevich, F. C. Lee, "An innovative technology for packaging power electronic building blocks using meandered interconnected parallel plate structures," *IEEE Trans. Compon. Packag. Manuf. Technol.*, vol. 22, no. 2, pp. 136-144, May 1999.
- [45] B. Mouawad, J. Li, A. Castellazzi, C. M. Johnson, "Hybrid bridge package for high voltage application," in *International Symposium on Semiconductor Devices and IC's*, June 2016.
- [46] I. Yaqub, J. Li, C. M. Johnson, "Dependence of overcurrent modes of IGBT modules on interconnect technology," *Microelectron. Reliab.*, vol. 55, no. 12, pp. 2596-2605, Dec. 2015.
- [47] C. DiMarino, M. Johnson, B. Mouawad, J. Li, D. Boroyevich, R. Burgos, G.-Q. Lu, M. Wang, "Design of a novel, high-density, high-speed 10 kV SiC MOSFET module," *IEEE Energy Conversion Congress and Exposition*, Sept. 2017.
- [48] C. DiMarino, M. Johnson, B. Mouawad, J. Li, R. Skuriat, Wang, Y. Tan, G.-Q. Lu, D. Boroyevich, R. Burgos, "Fabrication and characterization of a high-power-density, planar 10 kV SiC MOSFET power module," in *International Conference on Integrated Power Electronics Systems*, Mar. 2018.
- [49] C. DiMarino, B. Mouawad, C. M. Johnson, M. Wang, Y. Tan, Q. Lu, D. Boroyevich, R. Burgos, "Design and experimental validation of a wire-bond-less 10 kV SiC MOSFET power module," submitted to *IEEE Journal of Emerging and Selected Topics in Power Electronics*, 2019.
- [50] Z. Zhang, C. M. Johnson, "Suppression of electromagnetic interference using screening and shielding techniques with switching cells," in *IEEE International Workshop on Integrated Power Packaging*, Apr. 2017.
- [51] E. Hoene, A. Ostmann, C. Marczok, "Packaging very fast switching semiconductors," in *International Conference on Integrated Power Electronics Systems*, Feb. 2014.

- [52] J. H. Fabian, S. Hartmann, A. Hamidi, "Analysis of insulation failure modes in high power IGBT modules," in *Industry Applications Society Annual Meeting*, pp. 799-805, Oct. 2005.
- [53] J. H. Fabian, S. Hartmann, A. Hamidi, "Partial discharge failure analysis of AlN substrates for IGBT modules," *Microelectron. Rel.*, vol. 44, pp. 1425-2430, 2004.
- [54] G. Mitic, G. Lefranc, "Localization of electrical-insulation-and partial-discharge failures of IGBT modules," *IEEE Trans. Ind. Appl.*, vol. 38, no. 1, pp. 175-180, Jan./Feb. 2002.
- [55] C. F. Bayer, E. Baer, U. Waltrich, D. Malipaard, A. Schletz, "Simulation of the electric field strength in the vicinity of metallization edges on dielectric substrates," *IEEE Trans. Dielectr. Electr. Insul.*, vol. 22, no. 1, pp. 257-265, Feb. 2015.
- [56] O. Hohlfeld, R. Bayerer, T. Hunger, H. Hartung, "Stacked substrates for high voltage applications," in *International Conference on Integrated Power Electronics Systems*, Mar. 2012.
- [57] H. Hourdequin, L. Laudebat, M.-L. Locatelli, P. Bidan, "Design of packaging structures for high voltage power electronics devices: electric field stress on insulation," in *IEEE International Conference on Dielectrics*, July 2016.
- [58] D. Frey, J. L. Schanen, J. L. Auge, O. Lesaint, "Electric field investigation in high voltage power modules using finite element simulations and partial discharge measurements," in *Industry Applications Society Annual Meeting*, Oct. 2003.
- [59] H. Reynes, C. Buttay, H. Morel, "Protruding ceramic substrates for high voltage packaging of wide bandgap semiconductors," in *IEEE Workshop on Wide Bandgap Power Devices and Applications*, Nov. 2017.
- [60] C. DiMarino, J. Wang, R. Burgos, D. Boroyevich, "A high-power-density, high-speed gate driver for a 10 kV SiC MOSFET module," in *IEEE Electric Ship Technologies Symposium*, Aug. 2017.
- [61] Electronic Concepts, "MP80 series metallized polypropylene," MP80 datasheet, Rev. 4. Available: <https://www.ecicaps.com/film-capacitors/mp80-series/>
- [62] A. Kadavelugu, S. Bhattacharya, S.-H. Ryu, E. Van Brunt, D. Grider, A. Agarawal, S. Leslie, "Characterization of 15 kV SiC n-IGBT and its application considerations for high power converters," in *IEEE Energy Conversion Congress and Exposition*, Sept. 2013.
- [63] D. Johannesson, M. Nawaz, K. Ilves, "Assessment of 10 kV, 100 A silicon carbide MOSFET power modules," *IEEE Trans. Power Electron.*, vol. 33, no. 6, pp. 5215-5225, June 2018.
- [64] IXYS, "High voltage IGBT for capacitor discharge applications", IXGF30N400 datasheet, 2009. Available: [http://ixapps.ixys.com/DataSheet/DS99978C\(IXGF30N400\).pdf](http://ixapps.ixys.com/DataSheet/DS99978C(IXGF30N400).pdf)
- [65] C. DiMarino, B. Mouawad, K. Li, Y. Xu, M. Johnson, D. Boroyevich, R. Burgos, "A wire-bond-less 10 kV SiC MOSFET power module with reduced common-mode noise and electric field," in *International Exhibition and Conference for Power Electronics, Intelligent Motion, Renewable Energy and Energy Management*, June 2018.
- [66] Doble Engineering Company, "Doble in-service testing & assessment PD-Smart partial discharge analyzer," PD-Smart datasheet, Mar. 2016.